Am J Physiol Heart Circ Physiol 299: H1728–H1735, 2010.
First published August 13, 2010; doi:10.1152/ajpheart.00495.2010.

Two-photon microscopy-guided femtosecond-laser photoablation of avian cardiogenesis: noninvasive creation of localized heart defects

Huseyin C. Yalcin, Akshay Shekhar, Nozomi Nishimura, Ajinkya A. Rane, Chris B. Schaffer, and Jonathan T. Butcher

Department of Biomedical Engineering, Cornell University, Ithaca, New York

Submitted 21 May 2010; accepted in final form 9 August 2010

Yalcin HC, Shekhar A, Nishimura N, Rane AA, Schaffer CB, Butcher JT. Two-photon microscopy-guided femtosecond-laser photoablation of avian cardiogenesis: noninvasive creation of localized heart defects. *Am J Physiol Heart Circ Physiol* 299: H1728–H1735, 2010. First published August 13, 2010; doi:10.1152/ajpheart.00495.2010.—Embryonic heart formation is driven by complex feedback between genetic and hemodynamic stimuli. Clinical congenital heart defects (CHD), however, often manifest as localized microtissue malformations with no underlying genetic mutation, suggesting that altered hemodynamics during embryonic development may play a role. An investigation of this relationship has been impaired by a lack of experimental tools that can create locally targeted cardiac perturbations. Here we have developed noninvasive optical techniques that can modulate avian cardiogenesis to dissect relationships between alterations in mechanical signaling and CHD. We used two-photon excited fluorescence microscopy to monitor cushion and ventricular dynamics and femtosecond pulsed laser photoablation to target micrometer-sized volumes inside the beating chick hearts. We selectively photoablated a small (~100 μm radius) region of the superior atrioventricular (AV) cushion in Hamburger-Hamilton 24 chick embryos. We quantified via ultrasound that the disruption causes AV regurgitation, which resulted in a venous pooling of blood and severe arterial constriction. At 48 h postablation, quantitative X-ray microcomputed tomography imaging demonstrated stunted ventricular growth and pronounced left atrial dilation. A histological analysis demonstrated that the laser ablation produced defects localized to the superior AV cushion: a small quasispherical region of cushion tissue was completely obliterated, and the area adjacent to the myocardial wall was less cellularized. Both cushions and myocardium were significantly smaller than sham-operated controls. Our results highlight that two-photon excited fluorescence coupled with femtosecond pulsed laser photoablation should be considered a powerful tool for studying hemodynamic signaling in cardiac morphogenesis through the creation of localized microscale defects that may mimic clinical CHD.

chick embryo; hemodynamics; surgery; valve defects; mechanics; animal model

MORPHOGENESIS OF THE embryonic heart is a complex and dynamic process in which the linear heart tube becomes a multichambered pumping organ. The underlying mechanisms by which this complex remodeling occurs are poorly understood. Several studies have cataloged the increasing hemodynamic burden over cardiac morphogenesis (15, 21) during which the heart grows over 100-fold in size (4). As a result of this changing hemodynamic environment, there are alterations in multiple mechanical signals (hydrostatic pressure, strain, fluid shear, etc.) in the heart. Such changes in mechanical stimuli have been shown to drive changes in cell function in adult cardiac cells (2, 5, 19), which suggests that they may influence morphogenesis in vivo. Hove et al. (14) demonstrated that dramatically reducing blood inflow to or outflow from the tubular zebrafish heart resulted in hearts formed with an abnormal third chamber, diminished looping, and impaired valve formation. Vermot et al. (26) showed that eliminating reversing flows by decreasing blood viscosity in zebrafish embryos resulted in abnormal valvulogenesis. Similarly, the ligation of vitelline veins in embryonic chicks causes perturbations to intracardiac blood flow patterns that lead to a spectrum of cardiac malformations, including ventricular septal defects, valve anomalies, and outflow tract malformations (12). Hall et al. (11) showed that conotruncal banding in chick embryo hearts causes conduction system abnormalities through an interference with Purkinje fibers differentiation. Collectively, these studies support the idea that deviations from normal hemodynamically driven mechanical signaling in embryonic hearts may be a major cause of congenital heart defects (CHD).

Well-controlled animal model systems are essential to dissect the potentially cyclic relationships between mechanical signaling and cardiac tissue assembly and remodeling. Avian embryos are a useful animal model system to study the progression of CHD because of the structural and functional similarities between avian and human hearts (7). One such well-studied avian heart defect model is the left atrial ligation (LAL), which constricts blood flow to the left ventricle (24). The resulting cardiac remodeling captures many features of hypoplastic left heart syndrome, including the left ventricular atrophy and valve atresia (8, 23). This model enables an in vivo investigation of mechanical perturbations on cardiogenesis. Unfortunately, these microsurgical perturbations do not accurately recapitulate what is thought to be the clinical course of this disease in humans, where hypoplastic left heart syndrome is thought to be caused by outflow constrictions and not inflow obstructions (10).

While previous models of CHD, like the LAL model, have contributed substantively to our understanding of embryonic heart development and malformation, the clinical translation of this knowledge has been impaired because of the challenges of isolating direct cause and effect relationships. A significant unmet challenge is to develop the means for experimental manipulation of specific tissue locations without causing global or even regional tissue trauma. We have recently determined that changes in cushion valve action, structural organization, and tissue biomechanics both influenced and were strongly influenced by the local hemodynamic environment (3), suggesting that there may be a reciprocal feedback between changes in cardiac hemodynamics and changes in valvular structure and function. Connecting such feedback to the underlying biological mechanisms of morphogenesis requires

Address for reprint requests and other correspondence: J. T. Butcher, Dept. of Biomedical Engineering, 304 Weill Hall, Cornell Univ., Ithaca, NY 14853 (e-mail: jtb47@cornell.edu).

new tools that allow a direct experimental manipulation of tissue on a micrometer scale with minimal collateral effects.

Recent advances in nonlinear optical technology have enabled the creation of micrometer-sized voids at depths approaching a millimeter beneath a tissue surface without a significant disturbance to the surrounding regions or the overlying tissue. In this method, high-energy ultrashort (femtosecond duration) laser pulses are tightly focused on the targeted structure. Nonlinear absorption of the laser energy by the tissue leads to ionization in a femtoliter volume at the focal point of the objective, causing tissue damage in a nearly spherical region as small as 1 μm^3 (27). Recently, this photoablation technique was integrated with multiphoton microscopy to simultaneously visualize and photodisrupt individual microvessels in rat brain parenchyma (22). Here we demonstrate the use of femtosecond pulsed laser photoablation (FPLP) in combination with multiphoton microscopy for noninvasive perturbation of embryonic development of chick embryos. We photoablated the surface of a single atrioventricular (AV) cushion without inducing any exsanguination. We demonstrated that this caused an impaired apposition of the cushions, causing a ventricular regurgitation that led to an altered cardiac morphogenesis compared with that in controls.

MATERIALS AND METHODS

Ex ovo culture and egg incubation. Fertile white Leghorn chicken eggs were incubated blunt-side up in a constant humidity incubator at 37.5°C with continuous rocking (model GB1, Avery Incubators, Hugo, CO). After 3 days incubation [Hamburger-Hamilton (HH) 19–20 chick embryos], the eggs were cracked into the ex ovo culture systems slightly modified from those previously described (1, 4, 20). The eggs were aseptically transferred to a polyurethane membrane (Saran Wrap), affixed circumferentially inside a plastic cup, which was partially filled with sterile water.

Embryo preparation. To visualize the vasculature of embryos via two-photon excited fluorescence (2PEF) microscopy, we injected ~0.5–1 μl fluorescein-conjugated dextran (2 MDa, 1% wt/vol in Earle balanced salt solution, Sigma-Aldrich) into the blood circulation. Glass capillary tubes (0.75 mm ID) were pulled and fashioned into bevel-tipped microneedles with ~20-μm tip diameter using a microforge (Glassworx, St. Louis MO). The needle was positioned above a minor vitelline vein (<100 μm diameter) using a micromanipulator (model M3301L, World Precision Instruments, Sarasota FL). Dye was slowly injected into the vasculature over 2 min. For visualization and perturbation of the AV cushion, the embryos were gently repositioned such that the left side was faced up. Dysmorphic or bleeding embryos were excluded and discarded.

2PEF microscopy. A custom-built 2PEF microscope (25) was modified to include a path for a FPLP laser beam as previously described (22) (Fig. 1). Briefly, laser pulses (Mira-HP, Coherent, or μ-Jewel FCPA, IMRA America) were tightly focused into the sample, and the focal position was scanned using galvanometric mirrors to form 2PEF images. The 2PEF was reflected by a dichroic mirror and relayed to photomultiplier tubes that allow only the fluorescence to reach the detector. A 0.28 numerical aperture, ×4 magnification air objective (Olympus), was used to obtain whole embryo and whole heart images. A 1.0 numerical aperture ×20 magnification water-immersion objective (Zeiss) was used for high-resolution imaging at 10 frames per second and photoablation. The cultured embryos were placed on the translational stage and kept at 37.5°C with a custom-built water circulation heater as shown in Fig. 1.

Femtosecond pulsed laser photoablation. An amplified laser system (Legend, Coherent, Santa Clara, CA) produces high-energy, 50-fs duration pulses at a 1-kHz repetition rate. This laser beam was integrated into the microscope beam path using a polarizing beam splitter and was focused in the center of the 2PEF imaging field (Fig. 1). In this study, we targeted the endocardial surface of the superior AV cushion. We used cushion motion to ensure that tissue disruption is on the endocardial surface rather than within the cushion. The ablation beam was positioned on the endocardial/lumen border when the cushion was open. A mechanical shutter with a 2-ms minimum opening time (Uniblitz, Rochester, NY) was used to control the number of pulses. The shutter was opened for 1 s while the AV cushions were open, thus allowing the cushion to close in the path of the ablation beam. We used neutral density filters to adjust the pulse energy applied.

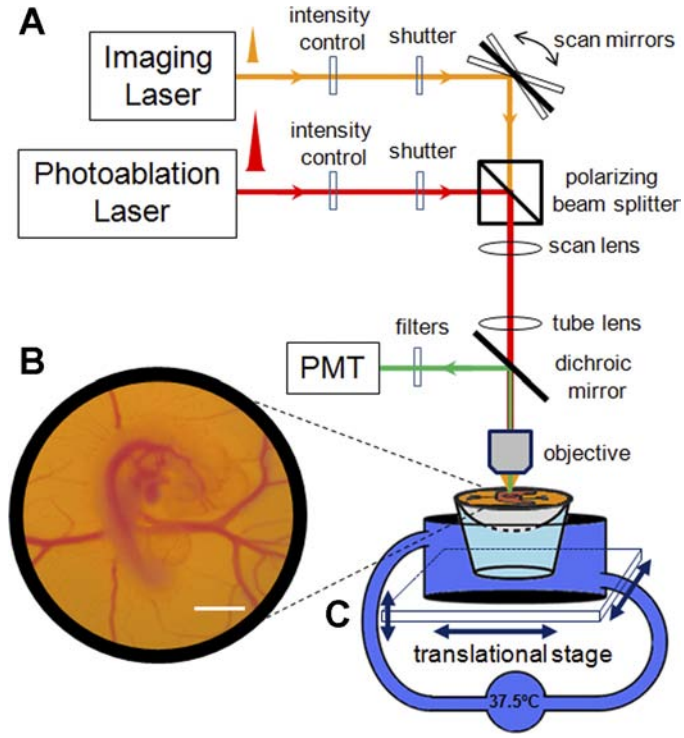

Fig. 1. Experimental setup. *A*: schematic of the two-photon excited fluorescence (2PEF) microscope modified for delivery of amplified ultrashort pulses for targeted photodisruption. *B*: bright-field image of ex ovo chicken embryo culture system. Scale bar = 2 mm. *C*: custom-heated circulation water bath used to maintain environmental conditions during imaging. PMT, photomultiplier tube.

Ultrasound imaging. Ultrasound imaging was performed to monitor hemodynamic changes postablation as previously described (3, 20). Imaging was performed using a RMV704 scan head on the Vevo770 high-frequency ultrasound system (VisualSonics, Toronto, Canada). The temperature of embryos during ultrasonography was closely monitored and kept constant at 37.5°C using the same water circulating heater shown in Fig. 1. For imaging, an aqueous contact zone was made between the ultrasound probe and the embryo using warmed Tyrode-HEPES solution. B-Mode and Doppler velocity profiles of the AV canal, ventricle, and proximal outflow were acquired according to our previously published techniques (3). Cardiac output and ejection fraction were quantified via the method of DeGroff (9). The ultrasound measurements were taken about 5 to 6 h after the photoablation experiments.

Three-dimensional stereology via microcomputed tomography. Microcomputed tomography (micro-CT) analysis was performed according to described protocols (4). Briefly, 50-μm glass microneedles were used to perfuse a polymerizing CT dense contrast agent microfil (Flow-Tech, Carver, MA) at a ratio of 20:75:5 (agent, diluent, and catalyst) through the ventricular apex region of HH27 chicks (48 h

after photoablation). Perfusion was controlled via gravity (20 cm height difference), which completely filled the cardiac chambers within 10 min. Microfil polymerized into a cast within 15 min, after which the entire embryo was fixed in 4% paraformaldehyde. Embryos were typically imaged within 48 h after fixation via micro-CT (eXplore CT 120, GE Healthcare) at a 25-μm voxel resolution. Datasets were processed using Microview (GE Healthcare) and Osirix (Osirix). Individual chamber volumes were segmented and quantified as previously described (4).

Histology/immunohistochemistry. Additional embryos were fixed 48 h after cushion ablation (HH27) with 4% paraformaldehyde, paraffin processed, and cut into 10-μm saggital sections. The sections were stained with hematoxylin and eosin to compare the general morphology and cellularity between treatments. Draq5 staining (1:1,000, Alexis Biochemicals, San Diego, CA) was applied as a nuclear counterstain control, whereas fluorescent antibody detection of α-smooth muscle actin (α-SMA, 1:100, Spring Bioscience, Pleasanton, CA) was used to identify cells with a mesenchymal phenotype within the AV cushions.

Statistics. Student *t*-test was used to show significance between groups, with $P < 0.05$ denoting significance.

RESULTS

Three-dimensional visualization of deep tissues in chick embryos in vivo via multiphoton microscopy. An exogenous administration of FITC-dextran via vitelline vein injection enabled a stable fluorescent visualization of the entire cardiovascular system for at least 2 h. For HH24 embryos seen in Fig. 2, the normal developmental position, right-side up (Fig. 2*A*), enables the visualization of cardiac structures on the right side, including the proximal and distal outflow (Fig. 2*B*) and the right aortic arches (Fig. 2*D*). To access the structures on the left side of the heart, the embryos were surgically flipped. This position (Fig. 2*F*) enabled us to visualize the ventricles (Fig. 2*C*) and the AV channel (Fig. 2*G*). Major blood vessels that are positioned in the center of the embryo like the common cardinal vein (Fig. 2*E*) could be visualized in either orientation.

Targeted AV cushion photoablation caused localized tissue damage. AV cushion morphogenesis occurs concurrently with the transition in ventricular pumping function, with the abutting cushions providing the sole valve action. Therefore, we hypothesized that the targeted photoablation of one of these cushions would affect ventricular hemodynamics and downstream remodeling. The visualization of the AV cushion was accomplished by creating whole embryo maps as seen in Fig. 2*F* and aligning this region of interest to the middle of the imaging screen. High-resolution imaging was then obtained to noninvasively visualize AV cushion function in contrast-enhanced embryos (Fig. 3*A*, and supplemental video 1). The entire profile of the superior cushion (adjacent to the inner

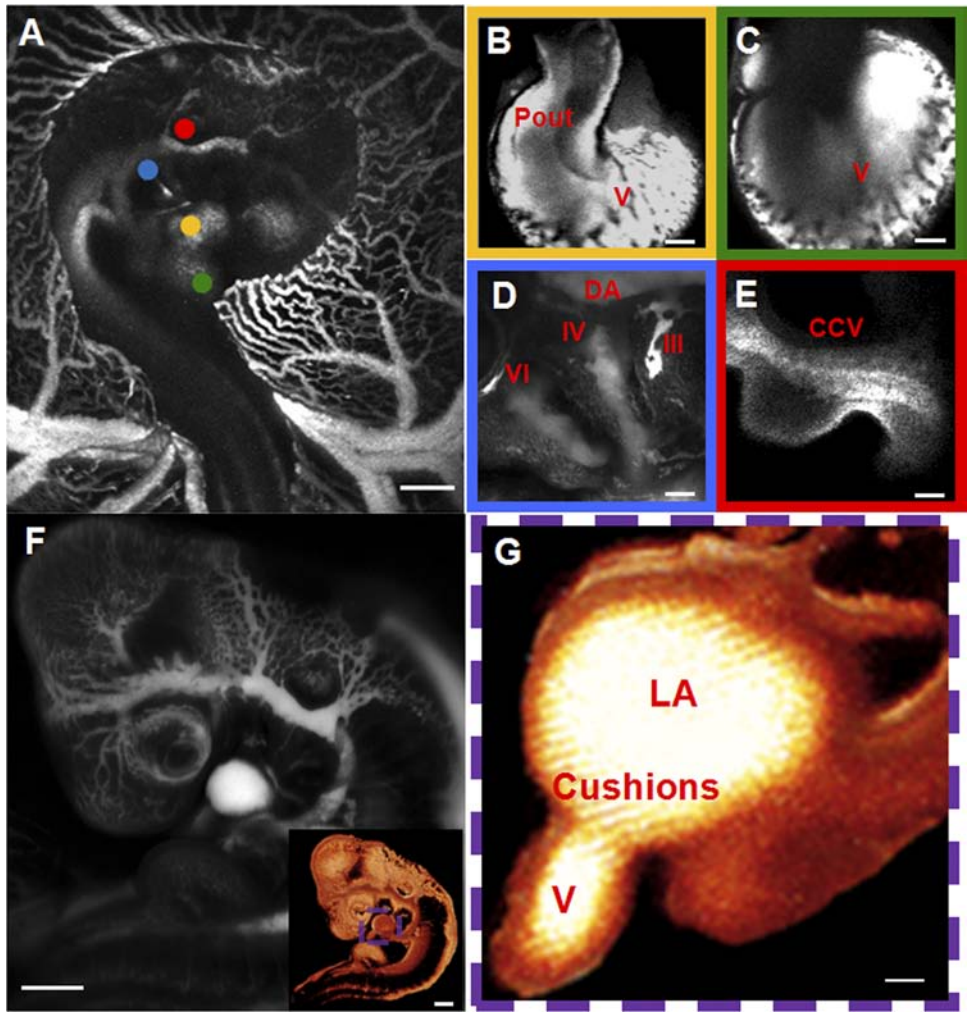

Fig. 2. 2PEF imaging of an Hamburger-Hamilton (HH) 24 chick embryo after intravenous injection of the fluorescent dye. *A*: normal developmental position of chick embryo (right-side up). *B*: proximal outflow (P_{out}). *C*: ventricles (V). *D*: aortic arches III, IV, and VI and dorsal aorta (DA). *E*: common cardial vein (CCV). *F*: flipped (left-side up) embryo. *Insert*: three-dimensional (3-D) computer reconstruction of flipped chick embryo. See supplemental video 3 for 360° rotation of a 3-D reconstructed image stack. *A–F*: average projections of 2PEF image stacks. *G:* left heart 3-D cross-section reconstruction for atrioventricular (AV) cushion visualization. LA, left atria. Box color surrounding the high-resolution in *B–E* matches dot colors in *A*, showing the location of the imaged region in the embryo. *G*: a digital cross section for region inside the colored dashed box in *F*. Scale bars: *A* and *F* = 1 mm; and *B–E* and *G* = 100 μm.

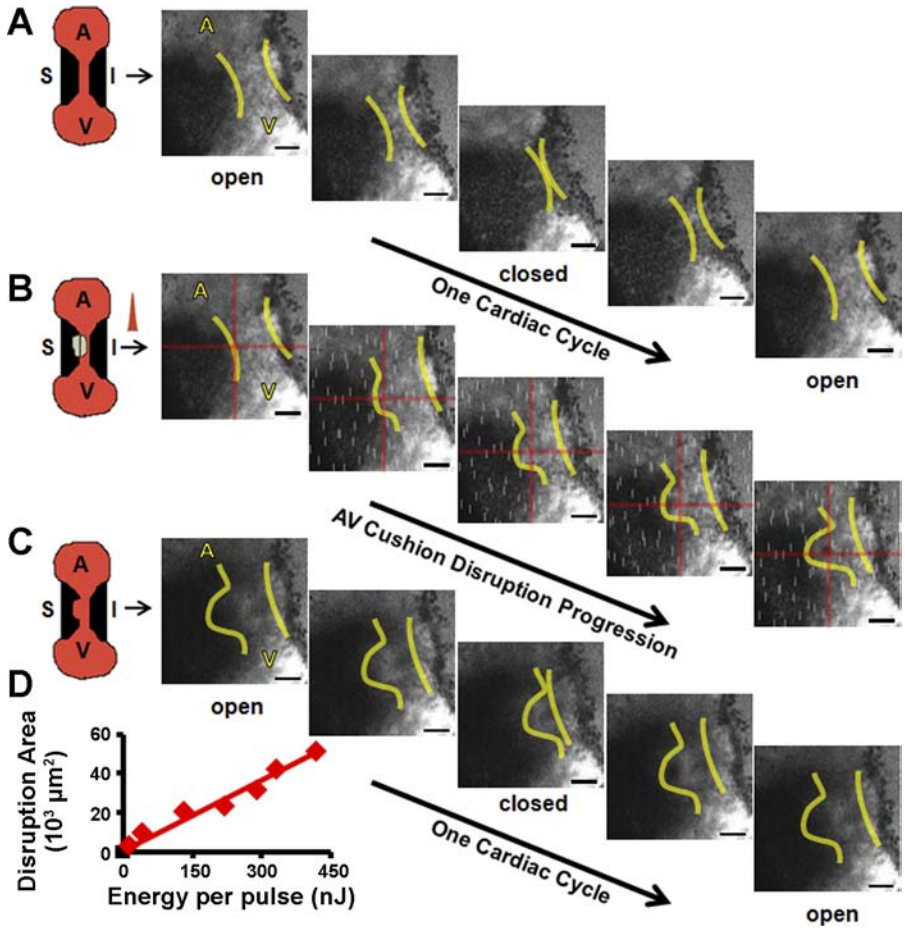

Fig. 3. HH24 AV cushion photoablation focused at crosshairs (red) for 1 s results in local tissue damage. Yellow lines indicate cushion boundaries: before (*A*), during (*B*), and after (*C*) photoablation. *A* and *C*: cushion motion during 1 cardiac cycle. White streaks in *B* are due to the ablation laser leaking through the filters on the detectors. A, atria; V, ventricle; S, superior AV cushion; I, inferior AV cushion (see supplemental video 2). Scale bar = 100 μm. *D*: AV cushion disrupted area, as measured from 2PEF images vs. incident laser energy. Trendline: linear regression ($y = 0.12x$, $R^2 = 0.957$).

curvature) was clearly visible during the entire cardiac cycle, whereas the inferior cushion was partially visible. Blood plasma was fluorescent, and circulating red blood cells appeared as dark discs. Dark granular material was also visible within the cushion via 2PEF microscopy. We presumed this represented cushion endocardial and mesenchymal cells. The fluorescence within the cushion suggests that the endocardial layer is partially permeable to the circulating dye at this stage. Positioning FPLP at the boundary of the open superior AV cushion resulted in a gradual tissue disruption as the cushions closed (Fig. 3*B*). FPLP was applied for 1 s. Permanent tissue damage was visually confirmed postablation (Fig. 3*C*). Energy per pulse was varied from 13.2 nJ, the lowest energy for visual damage, to 833 nJ, the largest energy before exsanguination. Disruption area was visually measured via 2PEF images (see supplemental video 2). A linear relationship was determined between the area of the AV cushion that was disrupted and incident laser energy (Fig. 3*D*), demonstrating our ability to control and optimize the insult that is produced.

Alteration in AV hemodynamics and cardiac function. Ultrasonography enabled real-time hemodynamic measurements to assess cardiac function. Acute changes in cardiac function because of targeted FPLP were quantified via Pulsed-Wave Doppler velocity measurement at the AV channel. Immediately after photoablation, reversed flow was observed from the ventricle to left atria during nearly 50% of the cardiac cycle (Fig. 4*A*). Photoablated embryos ($N = 7$) had a significant decrease in forward flow velocity (from 16.7 to 10.4 cm/s peak velocity, $P < 0.05$) and significant increase in reverse flow velocities (From 0 to 4.7cm/s peak velocity, $P < 0.05$) compared with sham controls ($N = 8$) (Fig. 4*A*). Cardiac output dropped by 19.8 μl/min, from 63.7 to 43.9 μl/min ($P = 0.005$), 31% difference and ejection fraction dropped by 13.4%, from 60.3% to 46.9% ($P = 0.003$), a 22% difference (Fig. 4*D*).

To create a reproducible AV regurgitation defect model, we characterized how the fraction of the cardiac cycle exhibiting reversed blood flow varied with the amount of valve cushion damage produced. We found that the fraction of the cardiac cycle showing backflow increased logarithmically with *1*) the incident laser energy and *2*) the area of the valve cushion that was disrupted (Fig. 4, *B* and *C*, respectively). These correlations enable the choice of ablation laser energy that produced significant but not immediately lethal regurgitation, 45 ± 5% of the cardiac cycle exhibiting reverse flow. Hearts remodeled rapidly at this magnitude (as described in *AV photoablation resulted in venous pooling and rapid cardiac remodeling*) and pumping efficiency decreased catastrophically as the embryo transitioned to a four-chamber configuration. Embryos were fixed after 48 h, which was before an expected demise 12–24 h later. We expect that lower degrees of induced regurgitation would have longer-term viability, but the focus of this experiment was to determine the consequences of AV regurgitation. About 200 nJ of incident energy per pulse was sufficient to induce adequate AV cushion tissue damage for this level of regurgitation, creating an ~100-μm radius spherical void in the superior AV cushion with no apparent damage to neigh-

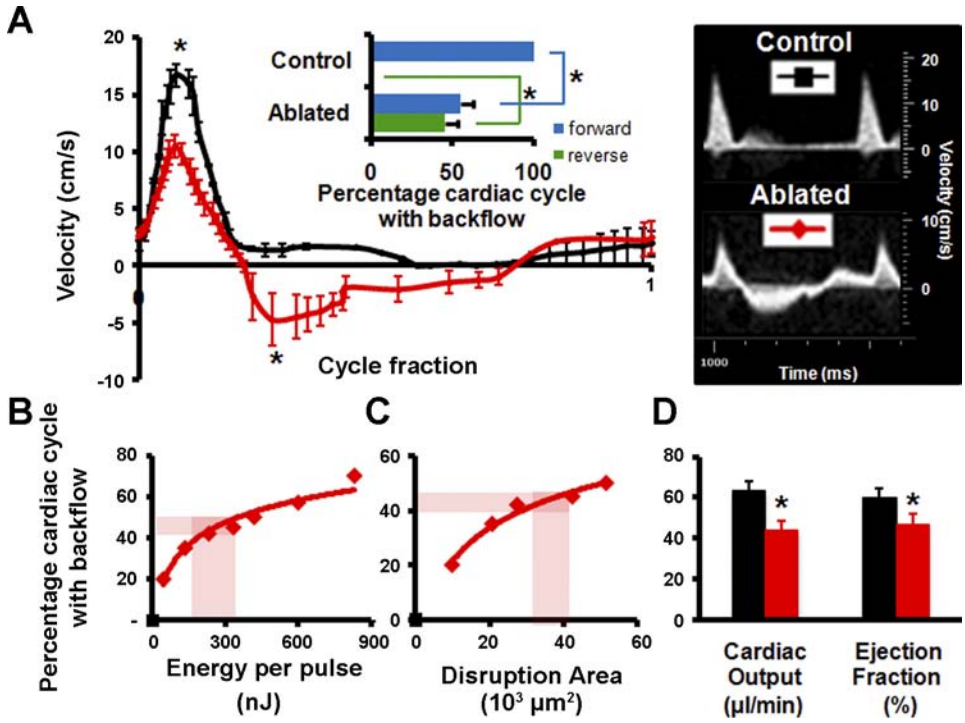

Fig. 4. Targeted HH24 AV cushion photoablation results in immediate ventricular regurgitation. *A*: Doppler ultrasound of AV cushion flow with and without ablation. *Inset*: quantification of forward and reverse flow at AV cushions (red, average ablated sample; and black, control). $*P < 0.05$. *B*: fraction of cardiac cycle with backflow, as measured with Doppler ultrasound, vs. incident laser energy. Trendline: logarithmic regression [$y = 15.3\ln(x) - 40$, $R^2 = 0.947$]. *C*: fraction of cardiac cycle with backflow vs. AV cushion disrupted area as measured from 2PEF images. Trendline: logarithmic regression [$y = 17.5\ln(x) - 19.5$, $R^2 = 0.992$]. Highlighted regions in *D* and *E* represent the energy for photoablation used in chronic studies, which results in reversed flow over ~45% of the cardiac cycle. *D*: ablated embryos ($N = 7$) have significantly decreased cardiac output and ejection fraction compared with normal ($N = 8$, $*P < 0.05$) (red, ablated; and black, control).

boring tissue (Fig. 3*C*). We verified via 2PEF and stereomicroscopy that no exsanguination occurred.

AV photoablation resulted in venous pooling and rapid cardiac remodeling. The severe regurgitation observed after targeted photoablation of the AV cushion caused blood to pool in the venous network. By 48 h, all veins were clearly visible and distended but arteries were significantly constricted, suggesting that the heart became extremely inefficient by that point (Fig. 5*A*). While the photoablation resulted in a stunted vascular development, anatomical developmental features such as cross-sectional areas for the eyes, wings, and legs were unaffected (Fig. 5*B*). We used micro-CT to quantify three-dimensional cardiac chamber growth in maximum diastolic distention (Fig. 5*C*) and observed significant dilation (19.5%) of the left atria and significant shrinkage of all other chambers (left ventricle, 24.8%; right ventricle, 18.3%; and right atria, 26.3%) for ablated embryos ($N = 6$) compared with controls ($N = 8$). Micro-CT analysis also revealed alterations in ventricular trabeculated structure, with less trabeculization for photoablated embryos.

Postmortem histological analysis. We qualitatively and quantitatively analyzed the morphology and cellular composition changes in cardiac structures after photoablation using histology and immunohistochemistry. Hematoxylin and eosin staining revealed that ablated embryos presented significantly smaller AV cushions (dashed yellow line) and myocardium (dashed red line, Fig. 6, *A* and *B*). A small (~100 μm radial) quasispherical region of the AV cushion of tissue was completely obliterated in the photoablation process (arrow in Fig. 6*A*). Cushion size decreased 39% ($P < 0.01$), and myocardium size decreased by 25% ($P < 0.05$). Sections of 50 μm on either side of the ablation showed no endocardial surface defect (not shown). The smaller cushions in the photoablated embryos also contained fewer cells than sham-operated controls. When normalized to cushion size and compared over the position from

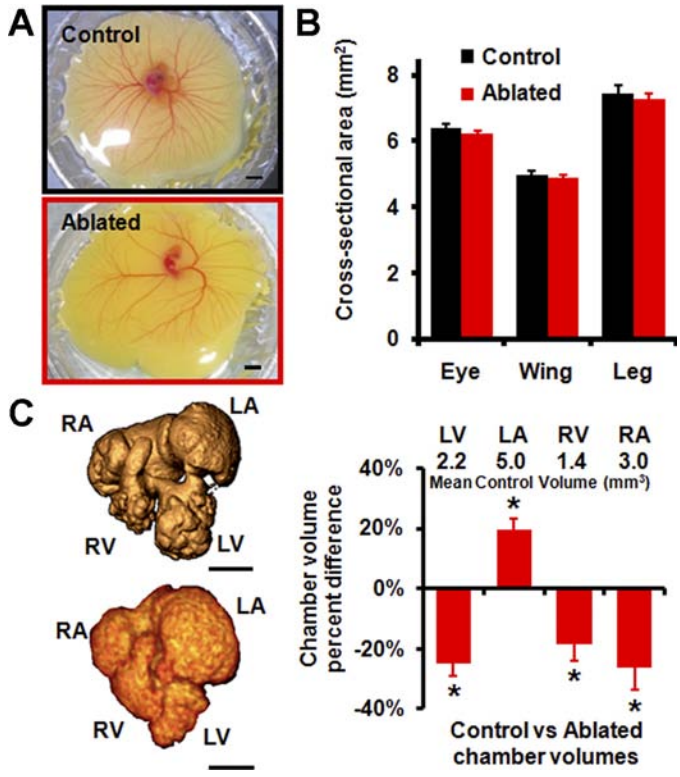

Fig. 5. Quantitative postmortem imaging of chick hearts 48 h after photoablation (HH27). *A*: at 48 h postphotoablation, ablated hearts show no exsanguination and induced regurgitation leads to venous pooling and stunted vascular development (red, ablated; and black, control). Scale bar = 5 mm. *B*: cross-sectional area of structures show no difference in noncardiovascular development ($N = 6$). *C*: 3-D microcomputed tomography imaging of control (*top*) and ablated (*bottom*) hearts reveals dilation of left atria (LA) and reduced growth of left ventricle (LV), right atria (RA), and right ventricle (RV). $*P < 0.05$; $N = 6$. Scale bar = 1 mm.

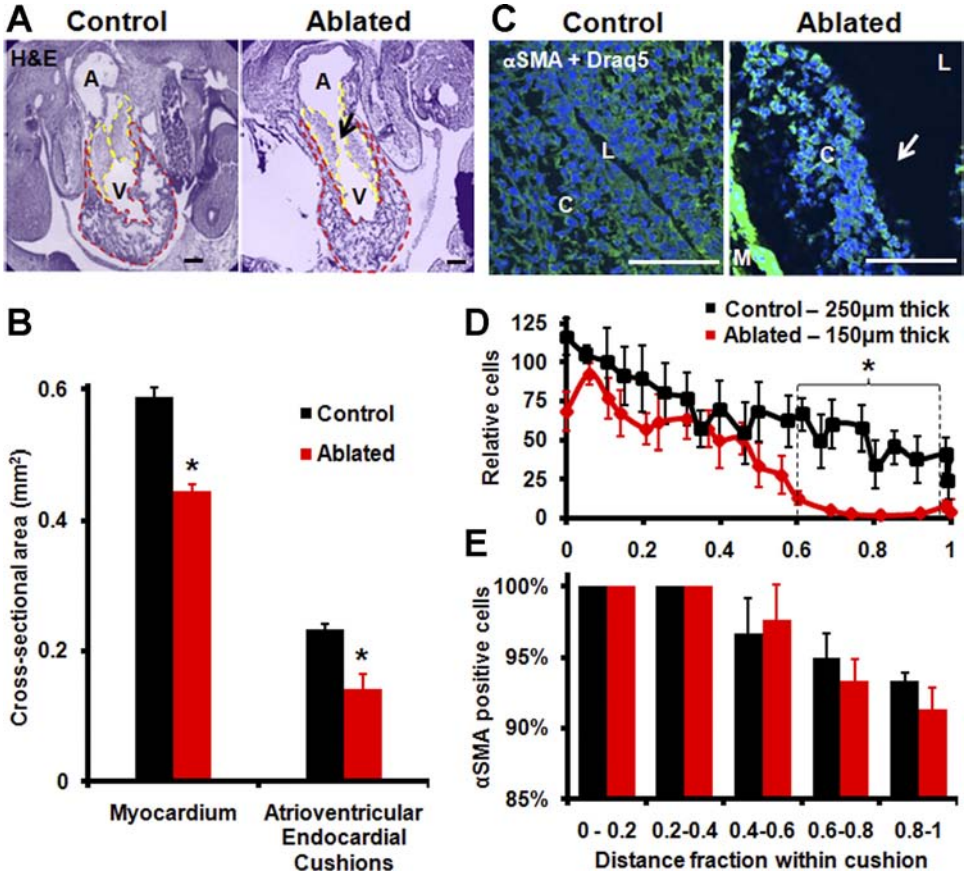

Fig. 6. Histological analysis of chick hearts 48 h postphotoablation (HH 27). *A*: hematoxylin and eosin (H&E) staining (purple) verifies changes in chamber dimensions with photoablation. Arrow indicates site of tissue disruption. Scale bar = 200 μm. *B*: ablated embryos have decreased myocardium and AV cushion cross-sectional area (*$P < 0.05$, $N = 8$). Areas analyzed are outlined in *A*: myocardium (red) and AV cushions (yellow). *C*: α-smooth muscle actin (α-SMA; green) and Draq5 (blue) staining of AV cushions. Arrow indicates site of tissue disruption. Scale bar = 100 μm. L, lumen; C, cushion; M, myocardium. *D*: average intensity value of α-SMA expression within AV cushions as a function of distance from the myocardium, normalized to the cushion thickness (*$P < 0.05$, $N = 8$). *E*: percentage of cells with α-SMA expression within AV cushions binned by distance from the myocardium ($N = 8$).

the lumen (L, 0) and myocardial border (M, 1), we found no significant differences in cell density at the cushion surface but almost no cells were found in the inner 40% of the AV cushion in ablated hearts (Fig. 6, *C* and *D*; $P < 0.05$). Interestingly, we found the same lack of cells and decreased cushion area in the contralateral nonablated cushion. α-SMA staining combined with Draq5 staining showed qualitative differences in the spatial distribution of labeled cells within the cushions (Fig. 6, *C* and *D*). Fewer cells migrated into the endocardial cushion matrix compared with sham-operated controls. We detected no difference in the percentage of α-SMA-positive cells at any depth within the cushions with either treatment (Fig. 6*E*). No difference was seen in the sarcomeric myosin expression (MF20, data not shown), indicating a mesenchyme-isolated patterning defect. Interestingly, these results were also found in the contralateral nonablated cushion.

DISCUSSION

Cardiogenesis and valvulogenesis are driven by both genetic and hemodynamic factors, alterations in which are root causes of CHD. There are limited numbers of in vivo CHD models incorporating altered hemodynamic environments because of the lack of techniques to precisely target cardiac structures without inducing severe global malformations. Here we used ultrashort high-energy laser pulses to induce spatially constrained tissue defects within avian embryo hearts to change the hemodynamic environment inside these hearts. The integration of this technique with multiphoton microscopy enabled us to simultaneously visualize and intervene inside the developing embryonic heart.

2PEF microscopy in vivo was used in this study. The technique offered a good alternative to other imaging in vivo modalities with higher resolution (13, 18, 20) and the ability to penetrate throughout the tissue of several hundred microns without bleaching or cytotoxicity (29). Limitations included a maximum imaging and ablation depth (~1.8 mm) and short-depth penetration because of tissue scattering (<1 mm), which prevented work with more mature embryos (>HH27). We were able to visualize a broad spectrum of extracardiac (arch arteries, dorsal aorta, and vitelline vessel network) and deep intracardiac structures (proximal and distal outflow, ventricles and endocardial cushions) in live chicks at high-spatial resolution (Fig. 2).

Current methods to mechanically perturb embryonic development employ invasive surgical procedures, including ligation (8), banding (6), transaction (16), microclips (12), and cautery (17). The results of these studies have highlighted the importance of hemodynamic signaling in cardiac morphogenesis. However, these techniques induce severe and large-scale disruptions that may not mimic all clinically relevant malformations. Therefore, noninvasive techniques are necessary since the most common cause of clinical CHD are defects to valvuloseptal structures that are formed by the cardiac cushions, but previous, surgically based approaches are not capable of targeted perturbation of deep intracardiac structures like ventricular septal walls or endocardial cushions.

One previous technique that overcomes these limitations is histotripsy, in which microbubbles created by ultrasound waves are used to damage tissue. The technique has been recently used to recapitulate an atrial septal defect in adult canine hearts (28).

This demonstrates the ability to visualize and disrupt structures beneath centimeters of tissue causing millimeter-size holes. In contrast, our method uses femtosecond duration pulsed laser energy, which is delivered to a targeted micrometer-sized volume inside the beating heart to cause localized tissue disruption through nonlinear optical absorption.

To test our approach, we decided to focus on an intracardiac region in which tissue alterations would lead to immediate hemodynamic changes. We focused femtosecond high-energy laser pulses at the AV cushion surface, which induced a localized disruption of the cushion, leading to an incomplete valve closure (Fig. 3). This, in turn, led to an immediate and pronounced regurgitation through the AV valve (Fig. 4), causing decreased cardiac function and leading to chamber remodeling over 48 h (Fig. 5). The degree of severity of the valve cushion damage (Fig. 3*D*) and therefore the acute changes in cardiac blood flow (Fig. 4, *B* and *C*) were easily tuned by adjusting the incident laser energy.

The cardiac remodeling quantified in this study was somewhat similar to the results from Sedmera et al. (24), who showed that decreased ventricular preload via LAL caused stunted left ventricular growth and altered myocardial trabeculation. The function of the cushions/valves in LAL-treated hearts has not been evaluated extensively, but the results suggest that these cushions remain thickened but do not regurgitate (8, 24). The permanent constriction of the left AV orifice in LAL likely effects more than just AV hemodynamics, including chamber growth and myocardial conduction patterns. It is unclear how these different effects can be isolated. In contrast to their study, however, we found smaller and less-cellularized AV cushions with targeted photoablation, which was a direct effect of both reduced ventricular preload (quantified by lower inflow velocity) and AV regurgitation. Collectively, these results suggest that endocardial cells are more sensitive to regurgitation than preload changes and that regurgitation is a much more serious problem for embryonic heart development. The ability to precisely control the location, amount of cushion ablation, and the degree of regurgitation with this technique enables a robust experimental analysis of the interactions between hemodynamics and biology in valvulogenesis.

In conclusion, 2PEF combined with FPLP is a powerful technique to simultaneously visualize and perturb embryonic morphogenesis. While the current application focused on AV cushion morphogenesis, the technique can be applied to any embryonic structure. The depth of penetration for both imaging and targeted ablation is ultimately limited by optical scattering, which for the wavelengths used here is about 1 mm in all areas of the embryo that we tested. Deep cardiac manipulation was possible with the current system up to stage HH27. Tools for localized noninvasive manipulation of embryonic development are critically needed to complement the significant molecular technologies available. A combination of these techniques will dramatically enhance our ability to dissect the complex and interrelated effects of genetic and hemodynamic signaling that likely drives clinical CHD.

ACKNOWLEDGMENTS

We thank Drew Noden, Mark Riccio, and Yung-Nung Chiu for technical assistance in this study. We thank Coherent and IMRA for the loan of lasers.

Present address of H. C. Yalcin: Mechanical Engineering Dept., Dogus Univ., Kadikoy 34722, Istanbul, Turkey.

GRANTS

This work was funded by American Heart Association Scientist Development Grant 0830384N (to J. T. Butcher), Scientist Development Grant 0735644T (to C. B. Schaffer), and Postdoctoral Fellowshhip 09POST2250177 (to N. Nishimura) and by a L'Oréal USA Fellowship for Women in Science (to N. Nishimura), a New York State Foundation Centers for Advanced Technology award (to J. T. Butcher), and the LeDucq foundation (Project MITRAL) (to J. T. Butcher).

DISCLOSURES

No conflicts of interest, financial or otherwise, are declared by the author(s).

REFERENCES

1. **Auerbach R, Kubai L, Knighton D, Folkman J.** A simple procedure for the long-term cultivation of chicken embryos. *Dev Biol* 41: 391–394, 1974.
2. **Butcher JT, Barrett BC, Nerem RM.** Equibiaxial strain stimulates fibroblastic phenotype shift in smooth muscle cells in an engineered tissue model of the aortic wall. *Biomaterials* 27: 5252–5258, 2006.
3. **Butcher JT, McQuinn TC, Sedmera D, Turner D, Markwald RR.** Transitions in early embryonic atrioventricular valvular function correspond with changes in cushion biomechanics that are predictable by tissue composition. *Circ Res* 100: 1503–1511, 2007.
4. **Butcher JT, Sedmera D, Guldberg RE, Markwald RR.** Quantitative volumetric analysis of cardiac morphogenesis assessed through micro-computed tomography. *Dev Dyn* 236: 802–809, 2007.
5. **Butcher JT, Tressel S, Johnson T, Turner D, Sorescu G, Jo H, Nerem RM.** Transcriptional profiles of valvular and vascular endothelial cells reveal phenotypic differences: influence of shear stress. *Arterioscler Thromb Vasc Biol* 26: 69–77, 2006.
6. **Clark EB, Hu N, Rosenquist GC.** Effect of conotruncal constriction on aortic-mitral valve continuity in the stage 18, 21 and 24 chick embryo. *Am J Cardiol* 53: 324–327, 1984.
7. **Cruz MD, Markward R.** *Living Morphogenesis of the Heart*: Boston: Birkhauser, 1998.
8. **deAlmeida A, McQuinn T, Sedmera D.** Increased ventricular preload is compensated by myocyte proliferation in normal and hypoplastic fetal chick left ventricle. *Circ Res* 100: 1363–1370, 2007.
9. **DeGroff CG.** Doppler echocardiography. *Pediatr Cardiol* 23: 307–333, 2002.
10. **Gomez-Fifer C.** Hypoplastic left heart syndrome in the fetus: Diagnostic features prior to birth and their impact on postnatal outcome. *Prog Pediatr Cardiol* 22: 53–60, 2006.
11. **Hall CE, Hurtado R, Hewett KW, Shulimovich M, Poma CP, Reckova M, Justus C, Pennisi DJ, Tobita K, Sedmera D, Gourdie RG, Mikawa T.** Hemodynamic-dependent patterning of endothelin converting enzyme 1 expression and differentiation of impulse-conducting Purkinje fibers in the embryonic heart. *Development* 131: 581–592, 2004.
12. **Hogers B, DeRuiter MC, Gittenberger-de Groot AC, Poelmann RE.** Unilateral vitelline vein ligation alters intracardiac blood flow patterns and morphogenesis in the chick embryo. *Circ Res* 80: 473–481, 1997.
13. **Hogers B, van der Weerd L, Olofsen H, van der Graaf LM, DeRuiter MC, Gittenberger-de Groot AC, Poelmann RE.** Non-invasive tracking of avian development in vivo by MRI NMR in biomedicine. *NMR Biomed* 22: 365–373, 2009.
14. **Hove JR, Koster RW, Forouhar AS, Acevedo-Bolton G, Fraser SE, Gharib M.** Intracardiac fluid forces are an essential epigenetic factor for embryonic cardiogenesis. *Nature* 421: 172–177, 2003.
15. **Hu N, Clark EB.** Hemodynamics of the stage 12 to stage 29 chick embryo. *Circ Res* 65: 1665–1670, 1989.
16. **Icardo JM.** Developmental biology of the vertebrate heart. *J Exp Zool* 275: 144–161, 1996.
17. **Jaffee OC.** Hemodynamic factors in the development of the chick embryo heart. *Anat Rec* 151: 69–75, 1965.
18. **Jenkins MW, Chughtai OQ, Basavanhally AN, Watanabe M, Rollins AM.** In vivo gated 4D imaging of the embryonic heart using optical coherence tomography. *J Biomed Opt* 12: 030505, 2007.
19. **MacKenna D, Summerour SR, Villarreal FJ.** Role of mechanical factors in modulating cardiac fibroblast function and extracellular matrix synthesis. *Cardiovasc Res* 46: 257–263, 2000.
20. **McQuinn TC, Bratoeva M, Dealmeida A, Remond M, Thompson RP, Sedmera D.** High-frequency ultrasonographic imaging of avian cardiovascular development. *Dev Dyn* 236: 3503–3513, 2007.

21. **Nakazawa M, Miyagawa S, Ohno T, Miura S, Takao A.** Developmental hemodynamic changes in rat embryos at 11 to 15 days of gestation: normal data of blood pressure and the effect of caffeine compared to data from chick embryo. *Pediatr Res* 23: 200–205, 1988.
22. **Nishimura N, Schaffer CB, Friedman B, Tsai PS, Lyden PD, Kleinfeld D.** Targeted insult to subsurface cortical blood vessels using ultrashort laser pulses: three models of stroke. *Nat Methods* 3: 99–108, 2006.
23. **Sedmera D, Cook AC, Shirali G, McQuinn TC.** Current issues and perspectives in hypoplasia of the left heart. *Cardiol Young* 15: 56–72, 2005.
24. **Sedmera D, Pexieder T, Rychterova V, Hu N, Clark EB.** Remodeling of chick embryonic ventricular myoarchitecture under experimentally changed loading conditions. *Anat Rec* 254: 238–252, 1999.
25. **Tsai PS, Frosting RD.** Principles, design and construction of a two-photon laser scanning microscope for in vitro and in vivo brain imaging. In: *In Vivo Optical Imaging of Brain Function.* Boca Raton: CRC, 2002, p. 113–171.
26. **Vermot J, Forouhar AS, Liebling M, Wu D, Plummer D, Gharib M, Fraser SE.** Reversing blood flows act through klf2a to ensure normal valvulogenesis in the developing heart. *PLoS Biol* 7: e1000246, 2009.
27. **Vogel A, Venugopalan V.** Mechanisms of pulsed laser ablation of biological tissues. *Chem Rev* 103: 577–644, 2003.
28. **Xu Z, Owens G, Gordon D, Cain C, Ludomirsky A.** Noninvasive creation of an atrial septal defect by histotripsy in a canine model. *Circulation* 121: 742–749, 2010.
29. **Zipfel WR, Williams RM, Webb WW.** Nonlinear magic: multiphoton microscopy in the biosciences. *Nat Biotechnol* 21: 1369–1377, 2003.